mathematics

Article

Dissipative Discrete PID Load Frequency Control for Restructured Wind Power Systems via Non-Fragile Design Approach

Hanmei Zhou [1,2,*], Qishui Zhong [1,3], Shaoyu Hu [1,2], Jin Yang [1,2], Kaibo Shi [1,4,*] and Shouming Zhong [5]

1 The Yangtze Delta Region Institute (Huzhou), University of Electronic Science and Technology of China, Huzhou 313001, China
2 School of Aeronautics and Astronautics, University of Electronic Science and Technology of China, Chengdu 611731, China
3 Aircraft Swarm Intelligent Sensing and Cooperative Control Key Laboratory of Sichuan Province, Chengdu 611731, China
4 School of Information Science and Engineering, Chengdu University, Chengdu 610106, China
5 School of Mathematics Sciences, University of Electronic Science and Technology of China, Chengdu 611731, China
* Correspondence: 202122100220@std.uestc.edu.cn (H.Z.); shikaibo@cdu.edu.cn (K.S.)

Abstract: This article proposes a discrete proportional-integral-derivative (PID) load frequency control (LFC) scheme to investigate the dissipative analysis issue of restructured wind power systems via a non-fragile design approach. Firstly, by taking the different power-sharing rates of governors into full consideration, a unified model is constructed for interconnected power systems containing multiple governors. Secondly, unlike existing LFC schemes, a non-fragile discrete PID control scheme is designed, which has the performance of tolerating control gain fluctuation and relieving the huge computational burden. Further, by constructing a discrete-type Lyapunov–Krasovskii functional, improved stability criteria with a strict dissipative performance index are established. Finally, numerical examples are presented to demonstrate the effectiveness of the proposed control method.

Keywords: discrete PID; LFC; non-fragile design approach; stability criteria; wind power system

MSC: 93D05

Citation: Zhou, H.; Zhong, Q.; Hu, S.; Yang, J.; Shi, K.; Zhong, S. Dissipative Discrete PID Load Frequency Control for Restructured Wind Power Systems via Non-Fragile Design Approach. *Mathematics* **2023**, *11*, 3252. https://doi.org/10.3390/math11143252

Academic Editor: Ivo Petráš

Received: 25 June 2023
Revised: 15 July 2023
Accepted: 16 July 2023
Published: 24 July 2023

1. Introduction

Load frequency control (LFC) is an important method for ensuring stability. The two main objectives of its implementation into interconnected power systems are maintaining the frequency and net power interchanges with neighboring areas at the scheduled values, by controlling the area control error (ACE) [1]. In recent years, due to changes in the power system environment and increased complexity and changes in the power system structure, each control area contains different kinds of uncertainties and various disturbances. Abrupt load changes can cause a mismatch between generation and demand, resulting in significant frequency deviations. Some relevant articles have studied the low-frequency oscillation issue of system states [2–4]. Therefore, to ensure competitiveness and efficiency in the electricity market, it is necessary to restructure the power system. Generation companies (GENCOs) can choose to participate or not in the task of LFC; there are more forms of cooperation between GENCOs and distribution companies (DISCOs), and any DISCO has the possibility of signing a contract with any GENCO under deregulation. Furthermore, the application of renewable energy is becoming increasingly widespread worldwide. Wind power, as an important renewable energy, makes a great contribution to energy conservation and emission reduction [5]. A restructured power system can help to increase the use of renewable energy sources. When a larger wind power generation replaces the conventional generator, the total inertia of the system decreases, and the equivalent regulation constant increases [6]. Some effective measures have been investigated to solve the previous problems. A novel scheme is developed for wind power modeling regardless of dependency distance in [7] to enhance the system's ability to handle the variability of wind generation. A supplement controller in a wind power control loop is designed to regulate the rotor speed [8] to remove the fluctuations in output wind power. A novel hidden Markov model is developed to obtain more accurate wind power forecast results [9] to guarantee a safe and reliable system operation. To enhance system damping, an optimized power point tracking controller was proposed [10]. To overcome the problem of high levels of wind power penetration, a model with DFIG-based wind turbines was constructed [11]. To counteract load fluctuations, a robust LFC scheme was designed [12]. Different from the methods mentioned above, the change in the active output in wind power is regarded as a load fluctuation, thus fully mobilizing the regulation capacity of conventional units by controlling the unstable frequency caused by the changes of loads and random fluctuations of wind power. A restructured LFC power system model with wind turbine generator sets is studied in this paper.

Designing suitable methods for LFC is of practical significance to minimize the ACE when load demands fluctuate, and various methods have been proposed in many studies, including a robust delay-dependent PI LFC scheme [13], an event-triggered PI control scheme [14], and a robust decentralized PI control scheme [15]. Considering the practical application, the PID control is more popular in the industry than PI control for its simple structure, strong robustness, and so forth [16]. Various approaches have been taken to design PID control in literature. Singh et al. [17] designed a PID controller with an optimum gain subject to linear matrix inequality (LMI) constraints. J.K. Pradhan and A. Ghosh designed a PID controller with multi-input and multi-output [18]. Pandey et al. [19] proposed a robust iterative PID control scheme. However, these control schemes are unable to deal with the uncertainties in the LFC model. Some researchers have used the non-fragile PID control to solve these problems [20,21]. Non-fragile discrete PID control is designed to provide robust performance by considering uncertainties and disturbances in the system. It can handle parameter variations and disturbances more effectively, leading to improved stability and performance compared to some existing LFC schemes. At the same time, it also limits its effectiveness in capturing complex nonlinear dynamics or dealing with highly uncertain systems for the reason that PID control is based on simple linear models. In addition, there are communication and computational burdens due to some microprocessors with limited computing abilities in the LFC scheme. Discrete control has been surveyed in some articles [22–24] because it relieves a huge computational burden and occupies smaller storage space. Therefore, a discrete PID controller is proposed with the time-windows of integral operation over a finite but adjustable length to relieve the computational burden. A non-fragile discrete PID control scheme is designed in this article to provide robust performance and save computing resources.

At present, the dissipativity theory has important applications in many topics such as robust control, regulation, and stabilization. Based on the input–output energy-related theory, strong links between physics and the control theory of systems are given by the dissipativity theory. In order to further analyze and design the control system, a framework is also provided [25]. A number of practical engineering systems have applied the dissipativity theory, for example, mechanical systems [26], robotic manipulators [27], and power systems [28,29]. Additionally, the dissipativity has also been applied in discrete-time networks [30,31] and continuous-time networks [32], respectively. The dissipative concept not only flexibly trades off gain and phase but also provides an appropriate framework for designing less conservative robust controls [33]. The results for a few LFC wind power systems motivated this study in which we consider the dissipative analysis for discrete-time interconnected systems. Dissipativity-based stability conditions consider the energy dissipation rates and their relationship with the system dynamics. By incorporating the dissipative behavior of the system, dissipativity-based stability criteria can capture stability properties more accurately and efficiently, resulting in reduced conservatism [34].

In this work, the main contributions can be summarized as the following three aspects:

1. A restructured wind power system model is introduced. Compared to some existing models, including single-generator unit models [35], the proposed restructured model introduces new information signals and different controller participation coefficients, resulting in better grid reliability.
2. A non-fragile discrete PID control scheme for interconnected wind power systems is designed, which can tolerate control gain fluctuation and reduce huge computation costs.
3. Based on the constructed discrete Lyapunov–Krasovskii functional, strict dissipativity conditions were established for wind power systems. The results can be obtained with lower conservatism and higher computational efficiency.

Notations: $\mathbb{N}$ denotes the set of natural numbers; $\mathbb{N}^+$ denotes the set of positive numbers. Let $\mathbb{R}^n$ and $\mathbb{R}^{n\times m}$ represent the n-dimensional Euclidean space and the set of $m \times n$ real matrices, respectively. A^{-1} and A^{T} denote, respectively, the inverse and the transpose of the matrix A. $[\Omega_{ij}]_{n\times n}$ represents the matrix consisting of $n \times n$ blocks, and the block in ith row and jth column is Ω_{ij}. $\mathbf{0}_{m\times n}$ and $\boldsymbol{I}_{m\times n}$ denote the zero matrix and the identity matrix with dimensions of $m \times n$. $Q > 0$ means that Q is a positive symmetric definite. $\mathbb{E}\{\cdot\}$ stands for the expectation of the stochastic variable " $\cdot$ ", and col[ ] represents the column vector. Let diag$\{\cdot\}$ be a diagonal matrix, i.e., $\mathrm{diag}\{X\}_N = \mathrm{diag}\{\underbrace{X,\ldots,X}_{N}\}$.

2. Preliminaries

This section develops a model of restructured interconnected wind power systems based on a non-fragile discrete PID LFC scheme. In Section 2.1, a model of interconnected wind power systems is constructed. In Section 2.2, a method is investigated to turn the above-mentioned model into a non-fragile discrete model. The parameters involved in the system are defined in Table 1.

Table 1. Practical meaning of system parameters.

$T_{\mathrm{t}_{ni}}$	Speed governor time constants	$\Delta P_{\mathrm{tie}i}$	Total tie-lie power deviation
$T_{\mathrm{g}_{ni}}$	Turbine time constants	ΔP_{m_i}	Turbines mechanical output
R_{ni}	Governor droop characteristic	ΔP_{d_i}	Load demands
D_i	Load damping coefficient	Δf_i	Deviation of valve position
T_{ij}	Coefficient of tie line	$\Delta P_{\mathrm{loc}_i}$	Contracted local demand
T_{w_i}	Wind generator time constants	ΔP_{L_j}	Other contracted demand
β_i	System frequency response coefficient	ΔP_{v_i}	Governors output
M_i	Inertia constant	ΔP_{w_i}	Wind generator output
α_{ni}	Participation factors of generator	ACE_i	Area control error

2.1. Restructured LFC Wind Power System Model

Let us define the generation participation matrix (GPM), which shows the participation factor of each Genco in the considered control areas, and each control area is determined by a Disco. For a large-scale power system in Figure 1 with n Gencos, the GPM will have the following structure:

$$GPM = \begin{bmatrix} gpf_{11} & gpf_{12} & \cdots & gpf_{1(N-1)} & gpf_{1N} \\ gpf_{21} & gpf_{22} & \cdots & gpf_{2(N-1)} & gpf_{2N} \\ \vdots & \vdots & \vdots & \vdots & \vdots \\ gpf_{(n-1)1} & gpf_{(n-1)2} & \cdots & gpf_{(n-1)(N-1)} & gpf_{(n-1)N} \\ gpf_{n1} & gpf_{n2} & \cdots & gpf_{n(N-1)} & gpf_{nN} \end{bmatrix},$$

where gpf_{ij} refers to the generation participation factor and shows the participation factor of Genco i in the load following area j. Meanwhile, $\sum_{i=1}^{n} gpf_{ij} = 1$. From Figure 1, we can see that

$$w_{1i} = \Delta P_{\text{loc}_i} + \Delta P_{\text{d}i} \tag{1}$$

$$\Delta P_{\text{tie}_i} = \Delta P_{\text{tie}_i,\text{act}} - w_{2i}. \tag{2}$$

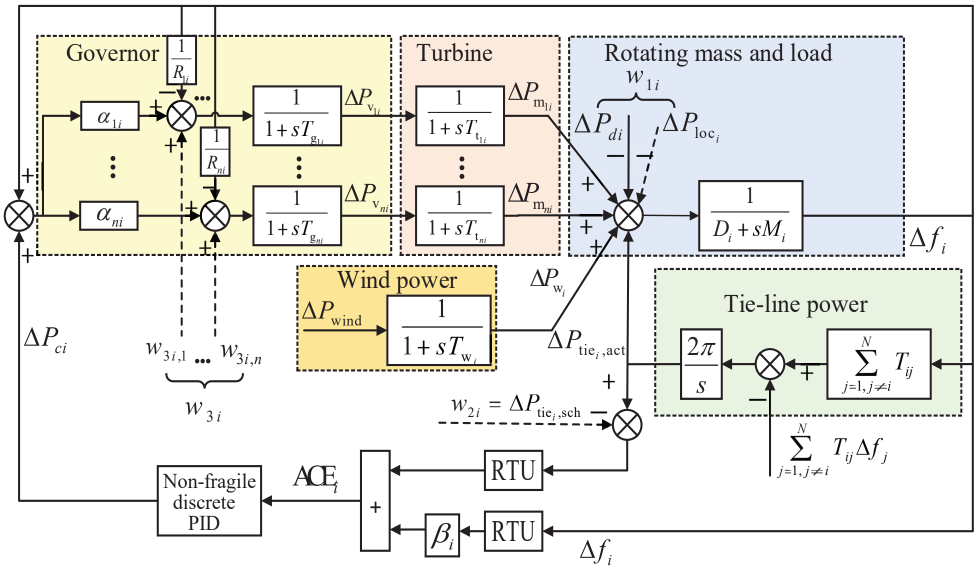

Figure 1. Interconnected LFC wind power system model.

We can obtain the following equations for the generalized scheduled w_{2i} and w_{3i}

$$w_{2i} = \sum_{j=1,j\neq i}^{N} (\sum_{k=1}^{n} gpf_{kj})\Delta P_{\text{L}j} - \sum_{k=1}^{n} (\sum_{j=1,j\neq i}^{N} gpf_{jk})\Delta P_{\text{L}i} \tag{3}$$

$$w_{3i,1} = \sum_{j=1}^{N} gpf_{1j}\Delta P_{\text{L}j}, \ \ldots, \ w_{3i,n} = \sum_{j=1}^{N} gpf_{nj}\Delta P_{\text{L}j}. \tag{4}$$

The total generation can be represented as

$$\Delta P_{mi} = \sum_{j=1}^{N} gpf_{ij}\Delta P_{\text{L}j}. \tag{5}$$

The model of ith area considering the wind power can be expressed as

$$\begin{cases} \Delta \dot{f}_i = \frac{1}{M_i}(\Delta P_{\text{m}_i} - \Delta P_{\text{d}_i} - \Delta P_{\text{tie}_i} - D_i \Delta f_i + \Delta P_{\text{w}_i}) \\ \Delta \dot{P}_{\text{tie}_i} = 2\pi \sum_{j=1,j\neq i}^{N} T_{ij}(\Delta f_i - \Delta f_j) \\ \Delta \dot{P}_{\text{v}_i} = A_{31_i}\Delta f_i + B_{3_i} u_i(t) + A_{33_i}\Delta P_{\text{v}_i} \\ \Delta \dot{P}_{\text{w}_i} = \frac{1}{T_{\text{w}i}}(\Delta P_{\text{wind}} - \Delta P_{\text{w}_i}) \\ \Delta \dot{P}_{\text{m}_i} = A_{23_i}\Delta P_{\text{v}_i} + A_{22_i}\Delta P_{\text{m}_i}. \end{cases} \tag{6}$$

Due to the presence of numerous components in the power system that introduce time delays, the inclusion of delay terms was considered in the model development to more accurately depict the dynamic behavior of the system. Define the following vectors

$$\Delta P_{\mathrm{v}_i}=\mathrm{col}[\Delta P_{\mathrm{v}_{1i}},\,\Delta P_{\mathrm{v}_{2i}},\,\ldots,\,\Delta P_{\mathrm{v}_{ni}}],\; w_i=\mathrm{col}[\Delta P_{\mathrm{wind}},\,\Delta P_{\mathrm{d}_i},\,\sum_{j=1,j\neq i}^{N}T_{ij}\Delta f_j]$$

$$\Delta P_{\mathrm{m}_i}=\mathrm{col}[\Delta P_{\mathrm{m}_{1i}},\,\Delta P_{\mathrm{m}_{2i}},\,\ldots,\,\Delta P_{\mathrm{m}_{ni}}],\; x_i=\mathrm{col}[\Delta f_i,\,\Delta P_{\mathrm{m}_i},\,\Delta P_{\mathrm{v}_i},\,\Delta P_{\mathrm{tie}_i},\,\Delta P_{\mathrm{w}_i}]$$

and $y_i=\mathrm{ACE}_i$, we arrive at

$$\begin{cases}\dot{x}_i(t)=A_ix_i(t)+B_iu_i(t)+A_{\tau_i}x_i(t-\tau_i(t))+\tilde{F}_iw_i(t)\\ y_i(t)=C_ix_i(t),\end{cases}\tag{7}$$

where

$$A_i=\begin{bmatrix}-\frac{D_i}{M_i} & A_{12_i} & \mathbf{0}_{1\times n} & A_{14_i}\\ \mathbf{0}_{n\times 1} & A_{22_i} & A_{23_i} & \mathbf{0}_{n\times 2}\\ A_{31_i} & \mathbf{0}_{n\times n} & A_{33_i} & \mathbf{0}_{n\times 2}\\ A_{41_i} & \mathbf{0}_{2\times n} & \mathbf{0}_{2\times n} & A_{44_i}\end{bmatrix},\; \tilde{F}_i=\begin{bmatrix}0 & -\frac{1}{M_i} & 0\\ \mathbf{0}_{2n\times 1} & \mathbf{0}_{2n\times 1} & \mathbf{0}_{2n\times 1}\\ 0 & 0 & -2\pi\\ \frac{1}{T_{\mathrm{w}i}} & 0 & 0\end{bmatrix},\; A_{44_i}=\begin{bmatrix}0 & 0\\ 0 & -1/T_{\mathrm{w}i}\end{bmatrix}$$

$$A_{41_i}=\begin{bmatrix}2\pi\sum_{j=1,j\neq i}^{N}T_{ij}\\ 0\end{bmatrix},\; A_{12_i}=\begin{bmatrix}1/M_i,\,\ldots,\,1/M_i\end{bmatrix},\; A_{33_i}=\mathrm{diag}\{-\frac{1}{T_{\mathrm{g}_{1i}}},\,\ldots,\,-\frac{1}{T_{\mathrm{g}_{ni}}}\}$$

$$A_{23_i}=-A_{22_i}=\mathrm{diag}\{\frac{1}{T_{\mathrm{t}_{1i}}},\,\ldots,\,\frac{1}{T_{\mathrm{t}_{ni}}}\},\; C_i=\begin{bmatrix}\beta_i & \mathbf{0}_{1\times 2n} & 1 & 0\end{bmatrix},\; A_{14_i}=\begin{bmatrix}-1/M_i,\,1/M_i\end{bmatrix}$$

$$A_{31_i}=\mathrm{col}\Big[-\tfrac{1}{T_{\mathrm{g}_{1i}}R_{1i}},\,\ldots,\,-\tfrac{1}{T_{\mathrm{g}_{ni}}R_{ni}}\Big],\; B_i=\mathrm{col}\Big[\mathbf{0}_{(n+1)\times 1},\,B_{3_i},\,0,\,0\Big],\; B_{3_i}=\mathrm{col}\Big[\tfrac{\alpha_{1i}}{T_{\mathrm{g}_{1i}}},\,\ldots,\,\tfrac{\alpha_{ni}}{T_{\mathrm{g}_{ni}}}\Big].$$

When taking into account the dotted line connections representing new load demands based on deregulated contracts, one can obtain that

$$\begin{cases}\Delta\dot{f}_i=\frac{1}{M_i}\left(\Delta P_{\mathrm{m}_i}+\Delta P_{\mathrm{w}_i}-\Delta P_{\mathrm{tie}_i}-D_i\Delta f_i-\Delta P_{\mathrm{tie}_i}-w_{1i}-w_{2i}\right)\\ \Delta\dot{P}_{\mathrm{tie}_i}=2\pi\sum_{j=1,j\neq i}^{N}T_{ij}\left(\Delta f_i-\Delta f_j\right)-w_{2i}\\ \Delta\dot{P}_{\mathrm{v}_i}=A_{31_i}\Delta f_i+B_{3_i}u_i(t)+A_{33_i}\Delta P_{\mathrm{v}_i}+F_{35_i}w_{3i}.\end{cases}\tag{8}$$

Define

$$\tilde{w}_i=\mathrm{col}\Big[\Delta P_{\mathrm{wind}},w_{1i},\textstyle\sum_{j=1,j\neq i}^{N}T_{ij}\Delta f_j,w_{2i},w_{3i}\Big],\; w_{3i}=\mathrm{col}\Big[w_{3i,1},\,w_{3i,2},\,\ldots,\,w_{3i,n}\Big]$$

we can obtain that

$$\begin{cases}\dot{x}_i(t)=A_ix_i(t)+B_iu_i(t)+A_{\tau_i}x_i(t-\tau_i(t))+F_i\tilde{w}_i(t)\\ y_i(t)=C_ix_i(t),\end{cases}\tag{9}$$

where

$$F_i=\begin{bmatrix}0 & -\frac{1}{M_i} & 0 & -\frac{1}{M_i} & 0\\ \mathbf{0}_{n\times 1} & \mathbf{0}_{n\times 1} & \mathbf{0}_{n\times 1} & \mathbf{0}_{n\times 1} & \mathbf{0}_{n\times 1}\\ \mathbf{0}_{n\times 1} & \mathbf{0}_{n\times 1} & \mathbf{0}_{n\times 1} & \mathbf{0}_{n\times 1} & F_{35i}\\ 0 & 0 & -2\pi & -1 & 0\\ \frac{1}{T_{\mathrm{w}_i}} & 0 & 0 & 0 & 0\end{bmatrix},\; F_{35_i}=\mathrm{col}\Big[\tfrac{1}{T_{\mathrm{g}_{1i}}},\,\ldots,\,\tfrac{1}{T_{\mathrm{g}_{ni}}}\Big].$$

2.2. Non-Fragile Discrete PID LFC Scheme

Different areas in interconnected LFC wind power systems are often associated with digital devices, which send discrete data to their neighboring areas. Define $T>0$ as the sampling interval. Then, one can obtain a discrete state-space model of multi-area as

$$\begin{cases} x_i(k+T) = \bar{A}_i x_i(k) + \bar{B}_i u_i(k) + \bar{A}_{\tau_i} x_i(k-\tau_i(k)) + \bar{F}_i w_i(k) \\ y_i(k) = \bar{C}_i x_i(k) \\ x_i(l) = \varphi_i(l),\ l = -\tau_M,\ -\tau_M+1,\ \dots,\ 0, \end{cases} \tag{10}$$

where $\bar{A}_i = e^{A_i T}$, $\bar{B}_i = \int_0^T e^{A_i t} B_i dt$, $\bar{A}_{\tau_i} = \int_0^T e^{A_i t} A_{\tau_i} dt$, $\bar{F}_i = \int_0^T e^{A_i t} F_i dt$, $\bar{C}_i = C_i$. $\tau_i(k)$ denotes the discrete time delay of the ith area.

Define $x(k) = \mathrm{col}[x_1(k),\ \dots,\ x_N(k)]$, $u(k) = \mathrm{col}[u_1(k),\ \dots,\ u_N(k)]$, $y(k) = \mathrm{col}[y_1(k), \dots, y_N(k)]$, and $w(k) = \mathrm{col}[\tilde{w}_1(k),\ \dots,\ \tilde{w}_N(k)]$. Then, a state-space representation of multi-area power systems can be expressed as

$$\begin{cases} x(k+1) = \bar{A}x(k) + \bar{B}u(k) + \bar{A}_\tau x(k-\tau(k)) + \bar{F}w(k) \\ y(k) = \bar{C}x(k) \\ x(l) = \varphi(l),\ l = -\tau_M,\ -\tau_M+1,\ \dots,\ 0, \end{cases} \tag{11}$$

where $\bar{A} = \mathrm{diag}\{\bar{A}_1,\ \dots,\ \bar{A}_N\}$, $\bar{B} = \mathrm{diag}\{\bar{B}_1,\ \dots,\ \bar{B}_N\}$, $\bar{C} = \mathrm{diag}\{\bar{C}_1,\ \dots,\ \bar{C}_N\}$, $\bar{A}_\tau = \mathrm{diag}\{\bar{A}_{\tau_1},\ \dots,\ \bar{A}_{\tau_N}\}$, $\bar{F} = \mathrm{diag}\{\bar{F}_1,\ \dots,\ \bar{F}_N\}$. $\tau(k) = \max\{\tau_i(k)\}$ $(i = 1, 2, \dots, N)$, and $\varphi(l)(l = -\tau_M,\ -\tau_M+1,\ \dots,\ 0)$ are the initial conditions.

Then, with the fluctuation in the gain matrices considered, a non-fragile LFC controller is designed as

$$u(k) = (K_\mathrm{P} + \alpha(k)\Delta K_\mathrm{P})y(k) + (K_\mathrm{I} + \beta(k)\Delta K_\mathrm{I})\sum_{l=k-m}^{k-1} y(l) + (K_\mathrm{D} + \lambda(k)\Delta K_\mathrm{D})(y(k) - y(k-1)), \tag{12}$$

where the change in proportion deviation can be calculated by ΔK_P, the change in integral deviation can be calculated by ΔK_I, and ΔK_D denotes the change in differential deviation. m is a known scalar representing the length of the time-windows, and it is assumed that $m \geq \tau_M$ in this paper. The mathematical characters $\alpha(k) \in \{0,1\}$, $\beta(k) \in \{0,1\}$, $\lambda(k) \in \{0,1\}$ are assumed to be known as

$$\mathbb{E}\{\varpi(k)\} = \varpi,\ \mathbb{E}\{(\varpi(k) - \varpi)^2\} = \varpi(1-\varpi)(\varpi \in \{\alpha,\ \beta,\ \lambda\}). \tag{13}$$

Define $\chi(k) = \mathrm{col}\Big[x(k-1),\ x(k-2),\ \dots,\ x(k-m)\Big]$, it follows from (11) that a discrete model can be expressed as

$$\begin{cases} x(k+1) = (\mathcal{A}_1 + \tilde{\alpha}(k)\mathcal{A}_2 + \tilde{\lambda}(k)\mathcal{A}_3)x(k) + (\mathcal{B}_1 + \tilde{\beta}(k)\mathcal{B}_2 - \tilde{\lambda}(k)\mathcal{B}_3)\chi(k) \\ \qquad\qquad + \bar{A}_\tau x(k-\tau(k)) + \bar{F}w(k) \\ y(k) = \bar{C}x(k) \\ x(l) = \varphi(l), l = -\tau_M,\ -\tau_M+1,\ \dots,\ 0, \end{cases} \tag{14}$$

where

$$\begin{aligned} &\mathcal{A}_1 = \bar{A} + \bar{B}(K_\mathrm{D} + K_\mathrm{P} + \bar{\lambda}\Delta K_\mathrm{D} + \bar{\alpha}\Delta K_\mathrm{P})\bar{C},\ \mathcal{A}_2 = \bar{B}\Delta K_\mathrm{P}\bar{C},\ \mathcal{A}_3 = \bar{B}\Delta K_\mathrm{D}\bar{C},\ \tilde{\lambda}(k) = \lambda(k) - \bar{\lambda}(k) \\ &\mathcal{B}_2 = \Big[\bar{B}\Delta K_\mathrm{I}\bar{C},\ \bar{B}\Delta K_\mathrm{I}\bar{C},\ \dots,\ \bar{B}\Delta K_\mathrm{I}\bar{C}\Big],\ \mathcal{B}_3 = \Big[\bar{B}\Delta K_\mathrm{D}\bar{C},\ 0,\ \dots,\ 0\Big],\ \tilde{\beta}(k) = \beta(k) - \bar{\beta}(k) \\ &\mathcal{B}_1 = \Big[\bar{B}(K_\mathrm{I} + \bar{\beta}\Delta K_\mathrm{I} - (K_\mathrm{D} + \bar{\lambda}\Delta K_\mathrm{D}))\bar{C},\ \bar{B}K_\mathrm{I}\bar{C},\ \dots,\ \bar{B}K_\mathrm{I}\bar{C}\Big],\ \tilde{\alpha}(k) = \alpha(k) - \bar{\alpha}(k) \\ &\Big[\Delta K_\mathrm{P},\ \Delta K_\mathrm{I},\ \Delta K_\mathrm{D}\Big] = \Xi \digamma(k)\Big[\beth_1,\ \beth_2,\ \beth_3\Big]. \end{aligned}$$

where Ξ and $\beth_\iota$ ($\iota = 1,\ 2,\ 3$) are the constant matrices, and $\digamma(k)$ is an indeterminate matrix constrained by $\digamma(k)\digamma^T(k) \leq I$. The discrete time delay $\tau(k)$ satisfies $\tau_m \leq \tau(k) \leq \tau_M$ $(k \in \mathbb{N}^+)$. τ_m represents the lower bound of $\tau(k)$, and τ_M represents the upper bound of $\tau(k)$, which are all known scalars.

Remark 1. *Multiple generation sets have been introduced into the interconnected wind power system to adjust the turbine input power, they decide the share of the load demands. In the reconstructed model, a reasonable power resource allocation scheme can balance the load requirements of the demand side and the supply side, and new information signals representing the power flow mobility between regions have been proposed, which can improve the efficiency and reliability of frequency regulation.*

Remark 2. *Notice that in the above discrete-time controller, three PID controller gain matrices,* K_{P}*,* K_{I}*, and* K_{D}*, are included. Current information and the trend in the information of outputs are well utilized with the introduction of the proportional terms* K_{P} *and differential terms* K_{D}*. Additionally, history measurements are fully used in the integral term* K_{I}*. In particular, compared with the continuous-time controller proposed in [36], a limited but adjusted length of time window is also designed in integral terms of discrete PID to relieve the computational burden.*

Remark 3. *Further, non-fragile control schemes are taken into account in the discrete PID controller in (12).* $\alpha(k)$*,* $\beta(k)$*, and* $\lambda(k)$ *describe the occurring status of the perturbation. When* $\alpha(k)$*,* $\beta(k)$*, and* $\lambda(k) = 0$*, it means that there is no proportion deviation. When* $\alpha(k)$*,* $\beta(k)$*, and* $\lambda(k) = 1$*, it means that there are multiplicative uncertainties being considered, which better explains the possible gain changes in the implementation process.*

Lemma 1 ([37])**.** *Given matrices* $Y > 0$*,* D*, and* E *with the appropriate dimensions, then*

$$Y + DF(k)E + E^{\mathrm{T}}F^{\mathrm{T}}(k)D^{\mathrm{T}} < 0 \tag{15}$$

for all $F(k)$ *satisfying* $F^{\mathrm{T}}(k)F(k) \leq I$*, if and only if there exists a scalar* $\xi DD^{\mathrm{T}} + \xi^{-1}E^{\mathrm{T}}E < 0$*.*

3. Results

Based on the model (14) proposed above, this section established dissipativity conditions in Theorem 1. Then, the control gain matrices based on a non-fragile discrete PID control scheme are designed in Theorem 2. This study aims to achieve an analysis of multi-area wind power systems, save limited network resources, and guarantee dissipative control. In the following, the definition of dissipativity is given.

Definition 1 ([30])**.** *System (14) is said to be strictly* (U_1, U_2, U_3)*-*γ*-dissipative if, for any* $\gamma > 0$*, such that*

$$\sum_{k=0}^{k^*} r(w(k), y(k)) \geq \gamma \sum_{k=0}^{k^*} w^{\mathrm{T}}(k)w(k),\ \forall k^* \geq 0 \tag{16}$$

holds under the zero initial condition. The energy supply rate function $r(w(k), y(k))$ *is defined as follows.*

$$r(w(k), y(k)) = y^{\mathrm{T}}(k)U_1 y(k) + 2y^{\mathrm{T}}(k)U_2 w(k) + w^{\mathrm{T}}(k)U_3 w(k), \tag{17}$$

where U_1*,* U_2*, and* U_3 *are real matrices with* $U_1 = U_1^{\mathrm{T}}$*,* $U_3 = U_3^{\mathrm{T}}$*, and* $U_1 \leq 0$*.*

Based on the discrete-type Lyapunov–Krasovskii functional, sufficient conditions for the control of system (14) are derived in the following theorem for given control feedback gains K_{P}, K_{I}, and K_{D}.

Theorem 1. *For a given integer* $\gamma > 0$*,* $\bar{\alpha} > 0$*,* $\bar{\lambda} > 0$*,* $\bar{\beta} > 0$*,* $\check{\alpha} > 0$*,* $\check{\lambda} > 0$*,* $\check{\beta} > 0$*,* $\tau_M > 0$*,* $\tau_m > 0$*,* ε_1*,* ε_2*, system (14) is strictly* (U_1, U_2, U_3)*-*γ*-dissipative, if there exist* $P > 0$*,* $Q_1 > 0$*,* $Q_2 > 0$*,* $Q_3 > 0$*,* $R > 0$ *and* $\daleth_1$*,* $\daleth_2$*,* $\daleth_3$*,* Ξ *of appropriate dimensions satisfying*

$$\Pi_1 = \begin{bmatrix} \Pi_1^{11} & * \\ \Pi_1^{21} & \Pi_1^{22} \end{bmatrix} < 0, \tag{18}$$

$$\Pi_2 = \begin{bmatrix} \Pi_2^{11} & * \\ \Pi_2^{21} & \Pi_2^{22} \end{bmatrix} < 0, \tag{19}$$

where

$$\Pi_1^{22} = -\text{diag}\{\text{P}\}_6,\ \Pi_2^{22} = -(1+1/\varepsilon_2)P,\ \check{\lambda} = \bar{\lambda}(1-\bar{\lambda}),\ \Pi_2^{21} = P\bar{F}$$

$$\varsigma = (2n+3)\times N,\ \Pi_2^{11} = \gamma I - U_3 - 1/\varepsilon_2 U_2,\ Q = \text{diag}\{Q_1,\ Q_2,\ \dots,\ Q_m\}$$

$$\check{\alpha} = \bar{\alpha}(1-\bar{\alpha}),\ \check{\beta} = \bar{\beta}(1-\bar{\beta}),\ \mathcal{P} = -P + \sum_{n=1}^{m} Q_n + (\tau_M - \tau_m + 1)R$$

$$\Pi_1^{11} = \begin{bmatrix} \mathcal{P} - \varepsilon_2 \bar{C}^T U_2 \bar{C} - \bar{C}^T U_1 \bar{C} & \mathbf{0}_{\varsigma\times\varsigma} & \mathbf{0}_{\varsigma\times\varsigma} \\ \mathbf{0}_{\varsigma\times\varsigma} & -Q & \mathbf{0}_{\varsigma\times\varsigma} \\ \mathbf{0}_{\varsigma\times\varsigma} & \mathbf{0}_{\varsigma\times\varsigma} & -R \end{bmatrix},\ \Pi_1^{21} = \begin{bmatrix} P\mathcal{A}_1 & P\mathcal{B}_1 & P\bar{A}_\tau \\ \sqrt{\varepsilon_1}P\mathcal{A}_1 & \sqrt{\varepsilon_1}P\mathcal{B}_1 & \sqrt{\varepsilon_1}P\bar{A}_\tau \\ \sqrt{\check{\alpha}}P\mathcal{A}_2 & \mathbf{0}_{\varsigma\times\varsigma} & \mathbf{0}_{\varsigma\times\varsigma} \\ \sqrt{\check{\lambda}}P\mathcal{A}_3 & \mathbf{0}_{\varsigma\times\varsigma} & \mathbf{0}_{\varsigma\times\varsigma} \\ \mathbf{0}_{\varsigma\times\varsigma} & \sqrt{\check{\beta}}P\mathcal{B}_2 & \mathbf{0}_{\varsigma\times\varsigma} \\ \mathbf{0}_{\varsigma\times\varsigma} & \sqrt{\check{\lambda}}P\mathcal{B}_3 & \mathbf{0}_{\varsigma\times\varsigma} \end{bmatrix}.$$

Proof of Theorem 1. Please see Appendix A. □

Remark 4. *In this paper, the discrete-type Lyapunov–Krasovskii functional is a mathematical function that assigns a scalar value to each state, which provides a systematic approach to analyze the stability of discrete-time wind power systems with higher computational efficiency. It is constructed based on the system dynamics and positive definiteness. The functional plays a crucial role in analyzing the stability and designing non-fragile discrete PID controllers for restructured wind power systems. We can see from the proof of Theorem 1 that the stability condition was derived based on the calculation of the forward difference $\Delta V(k)$, which deserves some comments. To bring the information of the delay into the final result, the Lyapunov–Krasovskii functional is chosen to be $V_3(k)$, and the calculation of $\Delta V_3(k)$ led to $\sum_{\rho=k-\tau(k+1)+1}^{k-1} x^{\mathrm{T}}(\rho)Rx(\rho)$, which was additionally introduced and gave rise to possible conservativeness. We have enlarged it to $\sum_{\rho=k-\tau(k+1)+1}^{k-\tau_m} x^{\mathrm{T}}(\rho)Rx(\rho)$ and $\sum_{\rho=k-\tau_m+1}^{k-1} x^{\mathrm{T}}(\rho)Rx(\rho)$ to reduce possible conservativeness.*

Remark 5. *It is worth mentioning that a strict $(U_1, U_2, U_3) - \gamma$ dissipative analysis problem is more general than some other problems. When $U_1 = -I$, $U_2 = 0$, and $U_3 = 2\gamma I$, the (U_1, U_2, U_3) dissipative properties degenerate into H_∞ properties strictly, which is shown by a dissipativity analysis. The dissipatiivity analysis in this paper is less conservative than H_∞ adopted for LFC of power system by most other studies.*

Theorem 2. *For a given integer $\gamma > 0$, $\bar{\alpha} > 0$, $\bar{\lambda} > 0$, $\bar{\beta} > 0$, $\check{\alpha} > 0$, $\check{\lambda} > 0$, $\check{\beta} > 0$, $\tau_M > 0$, $\tau_m > 0$, ε_1, ε_2, system (14) is strictly (U_1, U_2, U_3)-γ-dissipative, if there exist $\hat{P} > 0$, $\hat{Q}_1 > 0$, $\hat{Q}_2 > 0$, $\hat{Q}_3 > 0$, $\hat{R} > 0$ and $\beth_1$, $\beth_2$, $\beth_3$, Ξ of appropriate dimensions satisfying*

$$\Pi_3 = \begin{bmatrix} \Pi_3^{11} & * \\ \Pi_3^{21} & \Pi_3^{22} \end{bmatrix} < 0, \tag{20}$$

$$\tilde{\Pi}_2 = \begin{bmatrix} \tilde{\Pi}_2^{11} & * \\ \tilde{\Pi}_2^{21} & \tilde{\Pi}_2^{22} \end{bmatrix} < 0, \tag{21}$$

where

$$\Pi_3^{11} = \begin{bmatrix} \Phi_1 & * \\ \Phi_2 & \Phi_3 \end{bmatrix},\ \Phi_5 = \begin{bmatrix} \mathbf{0}_{N\times\varsigma} & \gimel_2 X & \gimel_2 X \\ \mathbf{0}_{N\times\varsigma} & \gimel_3 X & \mathbf{0}_{N\times\varsigma} \end{bmatrix},\ \Phi_2^{31} = \begin{bmatrix} (-U_1)^{\frac{1}{2}}\bar{C} \\ (-U_2)^{\frac{1}{2}}\bar{C} \end{bmatrix},\ \hat{\Xi} = \bar{B}\Xi\Xi^{\mathrm{T}}\bar{B}^{\mathrm{T}}$$

$$\gimel_1 = \daleth_1\bar{C},\ \Pi_3^{22} = \mathrm{diag}\{-\eta \boldsymbol{I}_{N\times N}\}_6,\ \Phi_1(3,3) = -\hat{R},\ \tilde{\Pi}_2^{22} = -(1+1/\varepsilon_2)\hat{P},\ \gimel_2 = \daleth_2\bar{C}$$

$$\Phi_1(1,1) = -\hat{P} + \sum_{n=1}^{m}\hat{Q}_n + (\tau_M - \tau_m + 1)\hat{R},\ \Phi_2^{13} = \begin{bmatrix} \bar{A}_\tau X & \sqrt{\varepsilon_1}\bar{A}_\tau X \end{bmatrix}^{\mathrm{T}},\ \gimel_3 = \daleth_3\bar{C}$$

$$\Phi_3 = \mathrm{diag}\{\Phi_3^1,\ -\hat{P},\ -\hat{P},\ -\hat{P},\ -\hat{P},\ \hat{U}_1\},\ \tilde{\Pi}_2^{21} = \bar{F},\ \hat{U}_1 = U_1{}^{-1},\ \Phi_1(2,2) = -\hat{Q}$$

$$\Phi_3^1 = \begin{bmatrix} -\hat{P}+\bar{\alpha}^2\hat{\Xi}+\bar{\lambda}^2\hat{\Xi} & \sqrt{\varepsilon_1}(\bar{\alpha}^2\hat{\Xi}+\bar{\lambda}^2\hat{\Xi}) \\ \sqrt{\varepsilon_1}(\bar{\alpha}^2\hat{\Xi}+\bar{\lambda}^2\hat{\Xi}) & -\hat{P}+\varepsilon_1(\bar{\alpha}^2\hat{\Xi}+\bar{\lambda}^2\hat{\Xi}) \end{bmatrix},\ \Pi_3^{21} = \begin{bmatrix} \Phi_4 & \mathbf{0}_{4N\times 3\varsigma} \\ \Phi_5 & \Phi_6 \end{bmatrix},\ \tilde{\Pi}_2^{11} = \gamma \boldsymbol{I}_{N\times N} - U_3$$

$$\Phi_6 = \begin{bmatrix} \gimel_2 X & \gimel_2 X & \gimel_2 X & \mathbf{0}_{N\times\varsigma} \\ \gimel_3 X & \mathbf{0}_{N\times\varsigma} & \mathbf{0}_{N\times\varsigma} & \mathbf{0}_{N\times\varsigma} \end{bmatrix},\ \Phi_4 = \begin{bmatrix} \gimel_3 X & \gimel_2 X \\ \gimel_1 X & -\gimel_3 X \\ \gimel_1 X & \mathbf{0}_{N\times\varsigma} \\ \gimel_3 X & \mathbf{0}_{N\times\varsigma} \end{bmatrix},\ \Phi_2 = \begin{bmatrix} \Phi_2^{11} & \mathbf{0}_{2\varsigma\times 2\varsigma} & \Phi_2^{13} \\ \mathbf{0}_{4\times\varsigma} & \mathbf{0}_{4\times 2\varsigma} & \mathbf{0}_{4\times\varsigma} \\ \Phi_2^{31} & \mathbf{0}_{N\times\varsigma} & \mathbf{0}_{N\times\varsigma} \end{bmatrix}$$

$$\Phi_2^{11} = \begin{bmatrix} \bar{A}X + \bar{B}Y_{\mathrm{D}} + \bar{B}Y_{\mathrm{P}} & \bar{B}\mathcal{Y} \\ \sqrt{\varepsilon_1}(\bar{A}X + \bar{B}Y_{\mathrm{D}} + \bar{B}Y_{\mathrm{P}}) & \sqrt{\varepsilon_1}\bar{B}\mathcal{Y} \end{bmatrix},\ \hat{Q} = \mathrm{diag}\{\hat{Q}_1,\ \hat{Q}_2,\ \ldots,\ \hat{Q}_m\}.$$

In addition, the PID control feedback gains are given by

$$K_{\mathrm{P}} = N_{\mathrm{p}}M_1{}^{-1},\ K_{\mathrm{I}} = N_{\mathrm{I}}M_1{}^{-1},\ K_{\mathrm{D}} = N_{\mathrm{D}}M_1{}^{-1}. \tag{22}$$

Proof of Theorem 2. Please see Appendix B. □

4. Illustrative Examples

In this section, the effectiveness of the model proposed in the above section are demonstrated in two parts. In Section 4.1, the effectiveness of the proposed control scheme is considered to be tested by two comparative simulation examples. In Section 4.2, the robustness of the proposed control scheme is validated by using various load disturbances.

4.1. Effectiveness of Non-Fragile Discrete PID LFC

Frequency deviation and tie-line power are key indicators of the system's response to load changes and generation imbalances. By analyzing the frequency deviation and tie-line power under different operating conditions and disturbances, we can assess the performance of the load frequency control. The goal is to keep the frequency and net power interchanges with neighboring areas at the scheduled values, typically around the nominal value. If the frequency deviations and tie-line power are small and quickly return to the nominal value after disturbances, it indicates effective load frequency control.

In this section, $\bar{\alpha} = 0.7$, $\bar{\beta} = 0.6$, and $\bar{\lambda} = 0.5$, which are the average success probabilities of the non-fragile items, and the trajectories of α, β, and λ are shown in Figure 2. The time length of the integral loop in the discrete PID controller (12) is taken as $m = 3$, the lower bound of the discrete time delay is taken as $\tau_m = 1$, and the upper bound is taken as $\tau_M = 3$.

Example 1 ([38]). *The parameters of the model (14) in two areas are listed in Table 2.*

Table 2. Parameters of two-area LFC scheme and each including two governors.

Parameters	T_t	T_g	R	D	β	M	α
Area 1	3.0	1.0	0.05	0.1884	21.0	0.1667	1.0
Area 2	4.0	1.7	0.05	0.1884	21.5	0.2084	1.0

The initial states in this example for two areas are defined as $x(-3) = x(-2) = x(-1) = x(0) = \begin{bmatrix} -4 & 4 & -5 & 5 & 2 \\ 1 & 1 & 2 & -2 & 4 \end{bmatrix}^{\mathrm{T}}$, and the fluctuation in the gain matrices of the non-fragile item in the control scheme of two areas are given as

$$\Delta K_{\mathrm{P}} = \begin{bmatrix} -1.8400 & -0.0400 \\ -0.8750 & -1.1250 \end{bmatrix}, \ \Delta K_{\mathrm{I}} = \begin{bmatrix} -0.2400 & -0.4400 \\ -0.3750 & -0.6250 \end{bmatrix}, \ \Delta K_{\mathrm{D}} = \begin{bmatrix} -0.4800 & -0.1000 \\ -0.6250 & -0.1875 \end{bmatrix}.$$

By solving LMI, the solution to matrix inequalities (A15) and (20) in Theorem 2 is computed. Then, the control gains of (14) for two areas are outlined as follows:

$$K_{\mathrm{P}} = \begin{bmatrix} 0.4770 & -0.0050 \\ 0.0008 & 0.4638 \end{bmatrix}, \ K_{\mathrm{I}} = \begin{bmatrix} 0.0005 & -0.0013 \\ -0.0012 & 0.0009 \end{bmatrix}, \ K_{\mathrm{D}} = \begin{bmatrix} 0.4770 & -0.0050 \\ 0.0008 & 0.4638 \end{bmatrix}.$$

In order to better demonstrate the effectiveness of the proposed non-fragile discrete PID in this paper, the responses of the system (14) are shown in Figures 3 and 4 for both the cases considering and not considering uncertainties. Additionally, Figures 5 and 6 describe the control inputs for the two operating conditions mentioned above. From Figures 3 and 4, it can be observed that the proposed non-fragile discrete PID control scheme operates stably and exhibits better control performance compared to other control schemes.

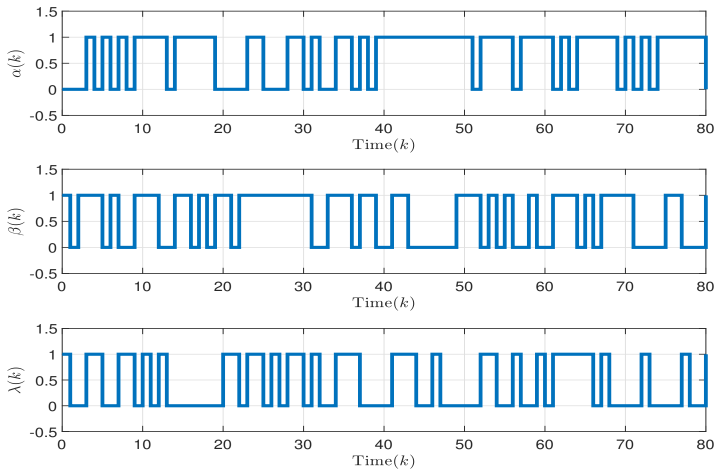

Figure 2. Trajectories of stochastic variable $\alpha(k)$, $\beta(k)$, $\lambda(k)$.

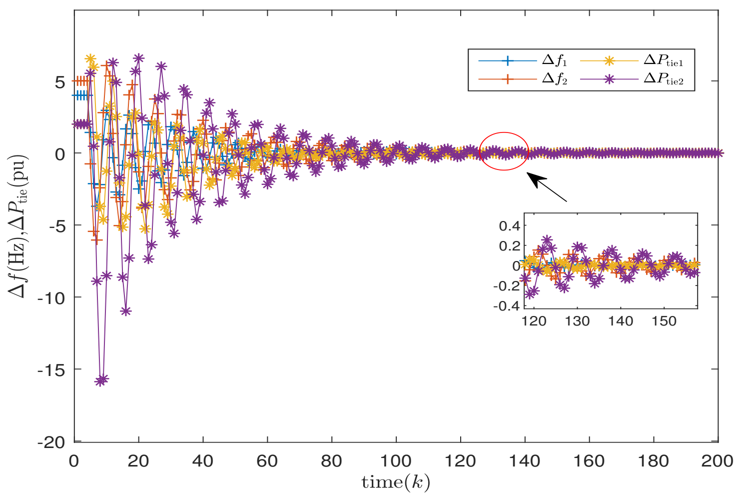

Figure 3. Frequency deviation and tie-line power of two areas considering uncertainties.

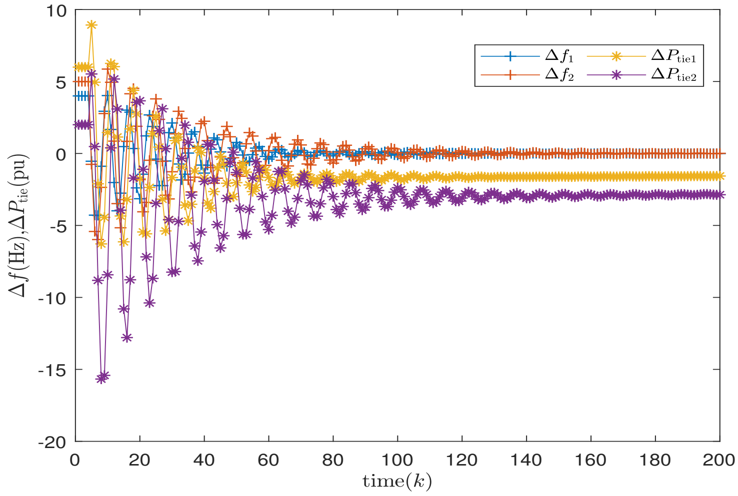

Figure 4. Frequency deviation and tie-line power of two areas without considering uncertainties.

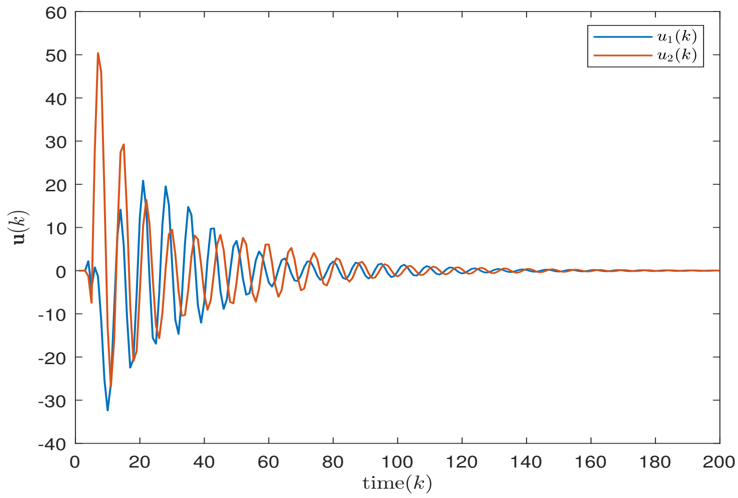

Figure 5. Control input of two areas considering uncertainties.

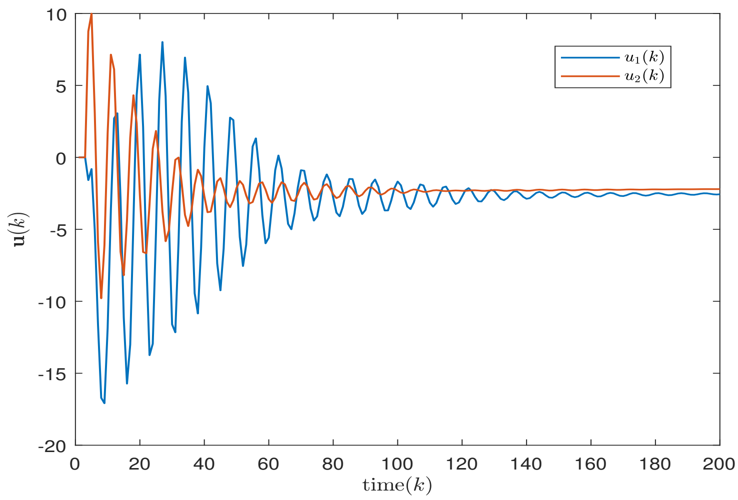

Figure 6. Control input of two areas without considering uncertainties.

Example 2 ([38]). *The parameters of the proposed model (14) in three areas are listed in Table 3.*

Table 3. Parameters of the three-area LFC scheme and each including two governors.

Parameters	**(k-i: kth Governor in ith Area)**					
	1-1	**2-1**	**1-2**	**2-2**	**1-3**	**2-3**
T_t	3.2	3	3	3.2	3.1	3.4
T_g	0.6	0.8	0.6	0.7	0.8	0.6
R	2.4	2.5	2.5	2.7	2.8	2.4
α	0.5	0.5	0.5	0.5	0.6	0.4

Parameters	Areas		
	1	2	3
M	0.1667	0.2084	0.1600
D	0.1884	0.1884	0.1780
β	0.4250	0.3966	0.3522
T_{ij}	T_{12} = 0.2450	T_{13} = 0.212	T_{23} = 0.11

The initial states in this example for three areas are defined as $x(-3) = x(-2) = x(-1) = x(0) = \begin{bmatrix} 4 & 4 & -5 & 5 & 2 & 2 & 2 \\ 5 & -4 & -5 & 5 & 2 & 2 & 2 \\ -4 & 4 & 4 & 5 & 2 & 3 & -2 \end{bmatrix}^{\mathrm{T}}$; the fluctuation in the gain matrices of the non-fragile item in the control scheme of three areas are given as

$$\Delta K_{\mathrm{P}} = \begin{bmatrix} -0.8800 & -0.0100 & -0.6400 \\ 0.0900 & -1.8650 & -0.2500 \\ -0.0100 & -0.2100 & -2.8500 \end{bmatrix}, \ \Delta K_{\mathrm{I}} = \begin{bmatrix} 0.020 & 0.370 & 0.210 \\ 0.315 & 0.035 & 0.230 \\ 0.260 & 0.360 & 0.020 \end{bmatrix}$$

$$\Delta K_{\mathrm{D}} = \begin{bmatrix} -0.8800 & -0.0750 & -0.3800 \\ 0.0900 & -1.8875 & -0.2500 \\ -0.0100 & -0.2750 & -1.9100 \end{bmatrix}.$$

Control gains of (12) for three areas are outlined as follows

$$K_{\mathrm{P}} = \begin{bmatrix} 0.9923 & -0.0846 & -0.1897 \\ -0.0032 & 0.9285 & -0.1846 \\ -0.0168 & -0.1236 & 0.9407 \end{bmatrix}, \ K_{\mathrm{I}} = \begin{bmatrix} 0.0135 & -0.0057 & -0.0015 \\ -0.0015 & 0.0100 & 0.0022 \\ -0.0001 & 0.0020 & 0.0055 \end{bmatrix}$$

$$K_{\mathrm{D}} = \begin{bmatrix} 0.9644 & 0.0534 & 0.1757 \\ -0.0046 & 1.0155 & 0.1810 \\ 0.0119 & 0.1164 & 1.0255 \end{bmatrix}.$$

In this case study, the effectiveness of the non-fragile control scheme was validated through an uncertainty analysis. The simulation results, as shown in Figures 7 and 8, depict the responses of the system (14) in three regions under both uncertain and certain conditions. The input trajectories of the controllers are illustrated in Figures 9 and 10. It is evident that under the design conditions of the non-fragile discrete PID, the system tends to stabilize and exhibits improved performance.

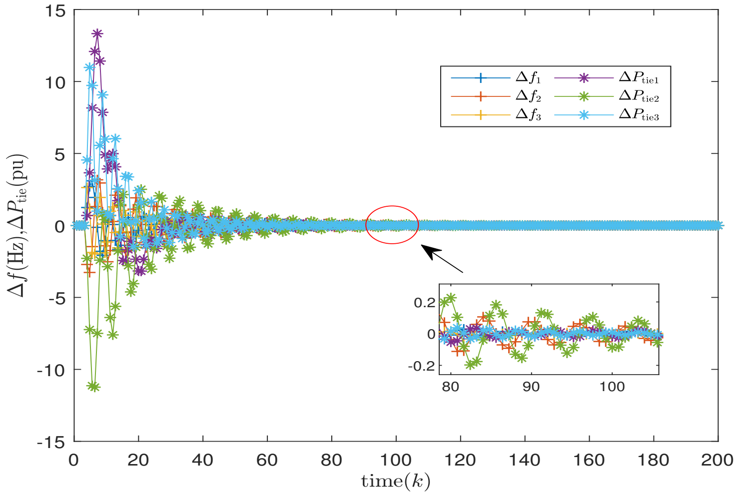

Figure 7. Frequency deviation and tie-line power of three areas considering uncertainties.

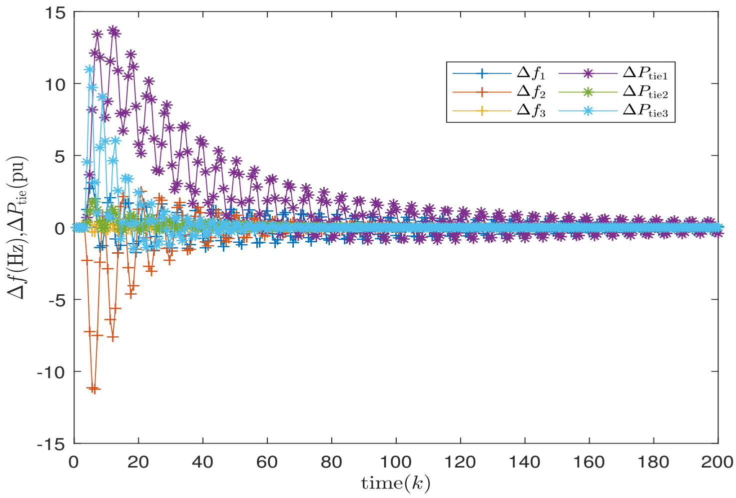

Figure 8. Frequency deviation and tie-line power of three areas without considering uncertainties.

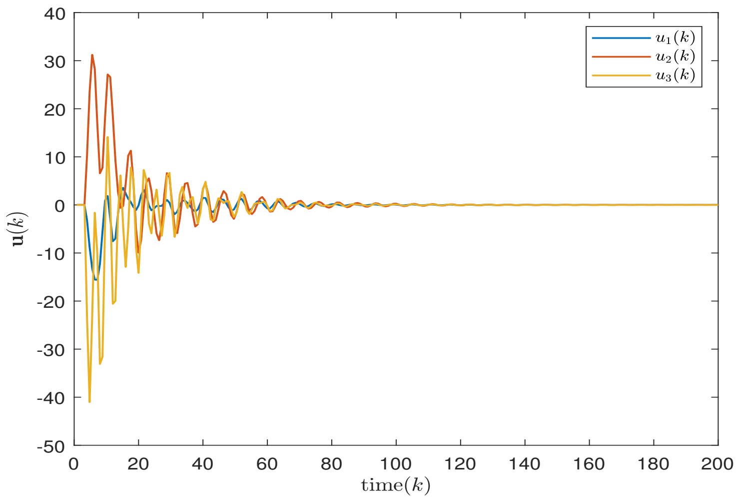

Figure 9. Control input of three areas considering uncertainties.

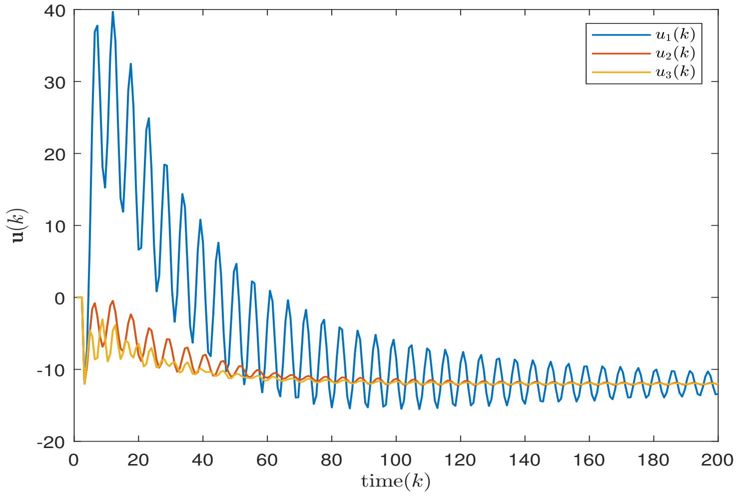

Figure 10. Control input of three areas without considering uncertainties.

4.2. *Case Study of Wind Power System*

Robustness assessment involves analyzing the performance of load frequency control under various operating conditions, parameter uncertainties, and disturbances. The control strategy demonstrates resilience and effectiveness in handling uncertainties and disturbances while maintaining system stability and desired frequency response. This section tests the system responses for different scenarios, including possible different bilateral contracts (GPM), wind power system is as shown in the Figure 11.

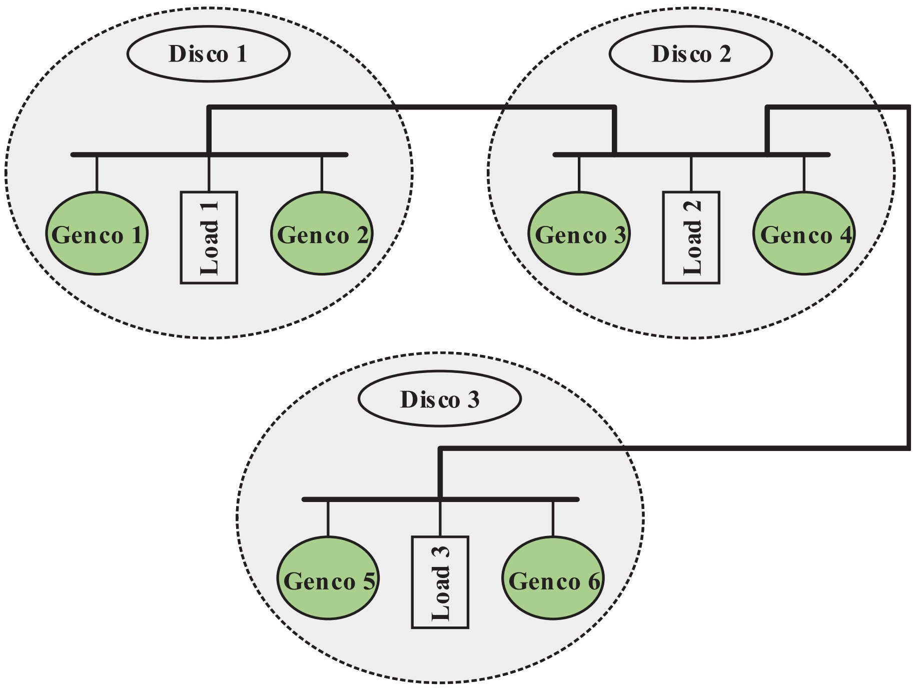

Figure 11. Wind power system of three areas.

Case 1: As the first test scenario, the following step load disturbances were applied to two areas: $\Delta P_{L_1}(k) = 100$ MW and $\Delta P_{L_2}(k) = 60$ MW. From $k = 0$ to $k = 200$, no disturbances were present in the system, and, at $k = 200$, a disturbance satisfying the previous condition was introduced. The GPM is given as follows:

$$GPM = \begin{bmatrix} 0.5 & 0 & 0 \\ 0.25 & 0 & 0 \\ 0 & 0.5 & 0 \\ 0 & 0.25 & 0 \\ 0 & 0 & 0.5 \\ 0 & 0 & 0.25 \end{bmatrix}.$$

As can be seen from Figure 12, the system finally reached stability under the conditions of Case 1.

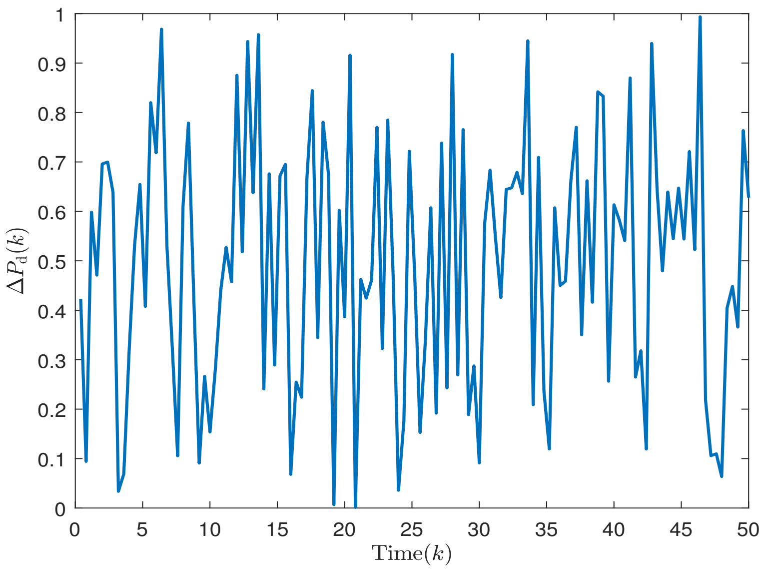

Figure 12. Trajectories of load disturbances.

Case 2: Generally, load disturbances in wind power systems are uncertain. Therefore, it is necessary to test the effectiveness of the controller considering randomly varying load disturbances. For simulation, the uncertainty of load disturbance for each region is calculated by using: $P_L(k) = R\cos(2\pi k)$, where R is a random number satisfying $R < 1$. The random load disturbance is shown in Figure 12, and it is applied in the system from $k = 600$. Given the signing rules between Discos and the available Gencos in other areas as the following GPM:

$$GPM = \begin{bmatrix} 0.25 & 0.25 & 0 \\ 0.5 & 0 & 0 \\ 0 & 0.25 & 0.75 \\ 0.25 & 0.25 & 0 \\ 0 & 0.25 & 0 \\ 0 & 0 & 0.25 \end{bmatrix}.$$

The simulation results confirm that the output signal eventually tends to zero, thus demonstrating the stability of the proposed system under random load disturbance.

The output signal of the area controlled can be seen in Figure 13, which indicates that the proposed control scheme can effectively achieve stability under various load fluctuations. The simulation results establish the efficacy of the suggested controller in moderating frequency deviation and tie-line power change in the restructured environment.

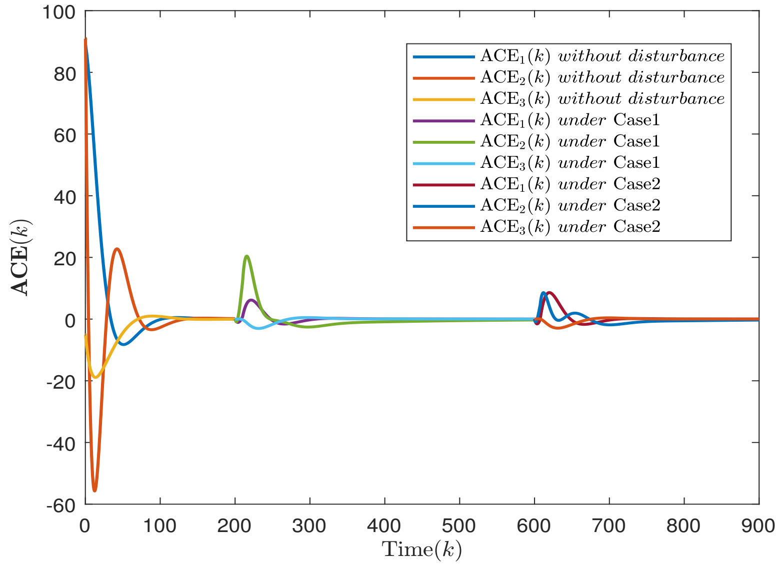

Figure 13. ACE of *i*th area under different load disturbances.

5. Conclusions

This paper has designed an LFC for reconstructed power systems containing multiple generation sets. Firstly, a restructured wind power system model has been introduced, which incorporated competition among market participants and provided a favorable environment for the integration of wind power into the grid to maintain grid reliability. Then, in order to relieve the computation burden of the system, a discrete PID control scheme has been designed. Moreover, considering the fluctuation in the gain matrices, the non-fragile model has been adopted to describe this phenomenon. Finally, two cases of wind power systems have been given to demonstrate the effectiveness of the proposed control approach under sufficient conditions to satisfy dissipativity. The proposed control scheme has also been verified by numerical examples.

Author Contributions: Conceptualization, H.Z., Q.Z., S.H., J.Y., K.S. and S.Z.; methodology, H.Z., Q.Z., S.H. and J.Y.; software, H.Z., Q.Z., S.H. and J.Y.; validation, Q.Z., K.S. and S.Z.; formal analysis, H.Z. and Q.Z.; investigation, H.Z., Q.Z., S.H. and J.Y.; resources, Q.Z. and K.S.; data curation, H.Z., Q.Z. and S.H.; writing—original draft preparation, H.Z.; writing—review and editing, H.Z., Q.Z., S.H., J.Y., K.S. and S.Z.; visualization, H.Z.; supervision, J.Y., K.S. and S.Z.; project administration, Q.Z., K.S. and S.Z. All authors have read and agreed to the published version of the manuscript.

Funding: This research was funded by the Sichuan Science and Technology Plan of funder grant number No. 2021ZDZX0003 and No.2022ZHCG0115; the China Postdoctoral Science Foundation of funder grant number No. 2020M683274 and No. 2021T140092; the Open Research Project of the State Key Laboratory of Industrial Control Technology, Zhejiang University, China, of funder grant number No. ICT2021B38; Guangdong Basic and Applied Basic Research Foundation of funder grant number No. 2021A1515011692; and the Program of Science and Technology of Sichuan Province of China of funder grant number No. 2021ZYD0012.

Data Availability Statement: The data presented in this study are available on request from the corresponding author.

Conflicts of Interest: The authors declare no conflict of interest. The funders had no role in the design of this study; in the collection, analyses, or interpretation of data; in the writing of the manuscript; or in the decision to publish the results.

Appendix A

Proof of Theorem 1. A discrete-type Lyapunov–Krasovskii functional is constructed to analyze the dissipativity of the system (14) as follows.

$$V(k) = \sum_{j=1}^{4} V_j(k), \tag{A1}$$

where

$$V_1(k) = x^{\mathrm{T}}(k)Px(k) \tag{A2}$$

$$V_2(k) = \sum_{n=1}^{m} \sum_{\rho=k-n}^{k-1} x^{\mathrm{T}}(\rho)Q_n x(\rho) \tag{A3}$$

$$V_3(k) = \sum_{\rho=k-\tau(k)}^{k-1} x^{\mathrm{T}}(\rho)Rx(\rho) \tag{A4}$$

$$V_4(k) = \sum_{s=k-\tau_M+1}^{k-\tau_m} \sum_{\rho=s}^{k-1} x^{\mathrm{T}}(\rho)Rx(\rho). \tag{A5}$$

By calculating the difference between $V(k)$ and taking the mathematical expectation along the trajectory of system (14), we have

$$\mathbb{E}\{\Delta V(k)\} = \sum_{j=1}^{4} \mathbb{E}\{\Delta V_j(k)\}, \tag{A6}$$

where

$$\begin{aligned}
&\mathbb{E}\{\Delta V_1(k)\} \\
=&\mathbb{E}\big\{(x^{\mathrm{T}}(k)(\mathcal{A}_1^{\mathrm{T}} + \tilde{\alpha}(k)\mathcal{A}_2^{\mathrm{T}} + \tilde{\lambda}(k)\mathcal{A}_3^{\mathrm{T}}) + \chi^{\mathrm{T}}(k)(\mathcal{B}_1^{\mathrm{T}} + \tilde{\beta}(k)\mathcal{B}_2^{\mathrm{T}} - \tilde{\lambda}(k)\mathcal{B}_3^{\mathrm{T}}) + x^{\mathrm{T}}(k-\tau(k))\bar{A}_\tau^{\mathrm{T}} \\
&+ w^{\mathrm{T}}(k)\bar{F}^{\mathrm{T}})P((\mathcal{A}_1+\tilde{\alpha}(k)\mathcal{A}_2+\tilde{\lambda}(k)\mathcal{A}_3)x(k)+(\mathcal{B}_1+\tilde{\beta}(k)\mathcal{B}_2-\tilde{\lambda}(k)\mathcal{B}_3)\chi(k)+\bar{A}_\tau x(k-\tau(k)) \\
&+ \bar{F}w(k)) - x(k)Px(k)\big\} \\
=&x^{\mathrm{T}}(k)(\mathcal{A}_1^{\mathrm{T}}P\mathcal{A}_1+\check{\alpha}\mathcal{A}_2^{\mathrm{T}}P\mathcal{A}_2+\check{\lambda}\mathcal{A}_3^{T}P\mathcal{A}_3-P)x(k)+\chi^{\mathrm{T}}(k)(\mathcal{B}_1^{\mathrm{T}}P\mathcal{B}_1 + \check{\beta}\mathcal{B}_2^{\mathrm{T}}P\mathcal{B}_2 + \check{\lambda}\mathcal{B}_3^{\mathrm{T}}P\mathcal{B}_3)\chi(k) \\
&+x^{\mathrm{T}}(k-\tau(k))\bar{A}_\tau^{\mathrm{T}}P\bar{A}_\tau x(k-\tau(k))+w^{\mathrm{T}}(k_T)\bar{F}^{\mathrm{T}}P\bar{F}w(k)+2x^{\mathrm{T}}(k)\mathcal{A}_1^{\mathrm{T}}P\mathcal{B}_1\chi(k)+2x^{\mathrm{T}}(k)\mathcal{A}_1^{\mathrm{T}}P\bar{F}w(k) \\
&+ 2x^{\mathrm{T}}(k)\mathcal{A}_1^{\mathrm{T}}P\bar{A}_\tau x(k-\tau(k)) +2\chi^{\mathrm{T}}(k)\mathcal{B}_1^{\mathrm{T}}P\bar{A}_\tau x(k-\tau(k))+2\chi^{\mathrm{T}}(k)\mathcal{B}_1^{\mathrm{T}}P\bar{F}w(k)+2x^{\mathrm{T}}(k-\tau(k)) \\
&\times \bar{A}_\tau^{\mathrm{T}}P\bar{F}w(k)
\end{aligned} \tag{A7}$$

$$\begin{aligned}
&\mathbb{E}\{\Delta V_2(k)\} \\
=&\mathbb{E}\Big\{\sum_{n=1}^{m}(\sum_{\rho=k+1-n}^{k} x^{\mathrm{T}}(\rho)Q_n x(\rho) - \sum_{\rho=k-n}^{k-1} x^{\mathrm{T}}(\rho)Q_n x(\rho))\Big\} \\
=&\sum_{n=1}^{m} \mathbb{E}\big\{x^{\mathrm{T}}(k)Q_n x(k) - x^{\mathrm{T}}(k-n)Q_n x(k-n)\big\}
\end{aligned} \tag{A8}$$

$$\begin{aligned}
&\mathbb{E}\{\Delta V_3(k)\} \\
=&\mathbb{E}\Big\{x^{\mathrm{T}}(k)Rx(k)-x^{\mathrm{T}}(k-\tau(k))Rx(k-\tau(k))+\sum_{\rho=k-\tau(k+1)+1}^{k-\tau_m} x^{\mathrm{T}}(\rho)Rx(\rho)-\sum_{\rho=k-\tau(k)+1}^{k-1} x^{\mathrm{T}}(\rho)Rx(\rho) \\
&+\sum_{\rho=k-\tau_m+1}^{k-1} x^{\mathrm{T}}(\rho)Rx(\rho)\Big\} \\
\leq&\mathbb{E}\Big\{x^{\mathrm{T}}(k)Rx(k) - x^{\mathrm{T}}(k-\tau(k))Rx(k-\tau(k) + \sum_{\rho=k-\tau_M+1}^{k-\tau_m} x^{\mathrm{T}}(\rho)Rx(\rho)\Big\}
\end{aligned} \tag{A9}$$

$$\begin{aligned}
&\mathbb{E}\{\Delta V_4(k)\}\\
=&\mathbb{E}\left\{\sum_{s=k-\tau_M+1}^{k-\tau_m}\sum_{\rho=s}^{k}x^{\mathrm{T}}(\rho)Rx(\rho)+\sum_{\rho=k-\tau_m+1}^{k}x^{\mathrm{T}}(\rho)Rx(\rho)-\sum_{\rho=k-\tau_M+1}^{k}x^{\mathrm{T}}(\rho)Rx(\rho)-\sum_{s=k-\tau_M+1}^{k-\tau_m}\sum_{\rho=s}^{k-1}x^{\mathrm{T}}(\rho)Rx(\rho)\right\}\\
=&\mathbb{E}\left\{\sum_{\rho=k-\tau_M+1}^{k-\tau_m}x^{\mathrm{T}}(k)Rx(k)-\sum_{\rho=k-\tau_M+1}^{k-\tau_m}x^{\mathrm{T}}(\rho)Rx(\rho)\right\}.
\end{aligned}\tag{A10}$$

Substituting (A7)–(A10) into (A6) leads to

$$\begin{aligned}
\mathbb{E}\{\Delta V(k)\}\leq{}&\Psi^{\mathrm{T}}(k)(\Theta_1+\Theta_2)\Psi(k)+w^{\mathrm{T}}(k)\bar{F}^{\mathrm{T}}P\bar{F}w(k)+2x^{\mathrm{T}}(k)\mathcal{A}^{\mathrm{T}}P\bar{F}w(k)+2\chi^{\mathrm{T}}(k)\mathcal{B}_1^{\mathrm{T}}P\bar{F}w(k)\\
&+2x^{\mathrm{T}}(k-\tau(k))\bar{A}_\tau^{\mathrm{T}}P\bar{F}w(k)\\
={}&\Psi^{\mathrm{T}}(k)(\Theta_1+\Theta_2)\Psi(k)+w^{\mathrm{T}}(k)\Theta_3w(k)+2\Psi^{\mathrm{T}}(k)\Theta_4w(k),
\end{aligned}\tag{A11}$$

where

$$\Psi(k)=\mathrm{col}\Big[x(k),\ \chi(k),\ x(k-\tau(k))\Big],\ \check{\mathcal{A}}_2=\mathcal{A}_2^{\mathrm{T}}P\mathcal{A}_2,\ \check{\mathcal{A}}_3=\mathcal{A}_3^{\mathrm{T}}P\mathcal{A}_3,\ \check{\mathcal{B}}_2=\mathcal{B}_2^{\mathrm{T}}P\mathcal{B}_2$$

$$\check{\mathcal{B}}_3=\mathcal{B}_3^{\mathrm{T}}P\mathcal{B}_3,\ \Theta_3=\bar{F}^{\mathrm{T}}P\bar{F},\ \Theta_1=\begin{bmatrix}\mathcal{P}+\check{\alpha}\check{\mathcal{A}}_2+\check{\lambda}\check{\mathcal{A}}_3 & * & *\\ 0 & -Q+\check{\beta}\check{\mathcal{B}}_2+\check{\lambda}\check{\mathcal{B}}_3 & *\\ 0 & 0 & -R\end{bmatrix}$$

$$\Theta_2=\begin{bmatrix}\mathcal{A}_1^{\mathrm{T}}P\mathcal{A}_1 & * & *\\ \mathcal{B}_1^{\mathrm{T}}P\mathcal{A}_1 & \mathcal{B}_1^{\mathrm{T}}P\mathcal{B}_1 & *\\ \bar{A}_\tau^{\mathrm{T}}P\mathcal{A}_1 & \bar{A}_\tau^{\mathrm{T}}P\mathcal{B}_1 & \bar{A}_\tau^{\mathrm{T}}P\bar{A}_\tau\end{bmatrix},\ \Theta_4=\begin{bmatrix}\mathcal{A}^{\mathrm{T}}P\bar{F}\\ \mathcal{B}_1^{\mathrm{T}}P\bar{F}\\ \bar{A}_\tau^{\mathrm{T}}P\bar{F}\end{bmatrix}.$$

Applying the elementary inequality $a^{\mathrm{T}}Pb+b^{\mathrm{T}}Pa\leq\varepsilon_1a^{\mathrm{T}}Pa+(1/\varepsilon_1)b^{\mathrm{T}}Pb$ (where a and b are vectors of compatible dimensions) to the term $2\Psi(k)\Theta_4w(k)$, one obtains

$$\begin{aligned}
2\Psi(k)\Theta_4w(k)={}&2x^{\mathrm{T}}(k)\mathcal{A}_1^{\mathrm{T}}P\bar{F}w(k)+2\chi^{\mathrm{T}}(k)\mathcal{B}_1^{\mathrm{T}}P\bar{F}w(k)+2x^{\mathrm{T}}(k-\tau(k))\bar{A}_\tau^{\mathrm{T}}P\bar{F}w(k)\\
\leq{}&\varepsilon_1\Psi^{\mathrm{T}}(k)\Theta_2\Psi(k)+1/\varepsilon_1w^{\mathrm{T}}(k)\Theta_3w(k).
\end{aligned}\tag{A12}$$

Then, it can be concluded from (A11) and (A12) that

$$\mathbb{E}\{\Delta V(k)\}\leq\tilde{\Psi}^{\mathrm{T}}(k)\Upsilon_1\tilde{\Psi}(k)+w^{\mathrm{T}}(k)\Upsilon_2w(k),\tag{A13}$$

where

$$\Upsilon_1=(1+\varepsilon_1)\Theta_2+\Theta_1,\Upsilon_2=(1+1/\varepsilon_1)\Theta_3.$$

By using the Schur complement, one can obtain

$$\begin{aligned}
\mathbb{E}\{\Delta V(k)\}\leq{}&\Psi^T(k)(\Pi_1^{11}-\Pi_1^{21\,T}\Pi_1^{22\,-1}\Pi_1^{21})\Psi(k)+w^T(k)(\Pi_2^{11}-\Pi_2^{21\,T}\Pi_2^{22\,-1}\Pi_2^{21})w(k)\\
&+r(w(k),y(k)-\gamma w^T(k)w(k).
\end{aligned}\tag{A14}$$

It can be seen that if (A14) satisfies the inequalities (18) and (19), we can draw the following conclusions

$$\mathbb{E}\{\Delta V(k)\}\leq r(w(k),y(k))-\gamma w^{\mathrm{T}}(k)w(k).\tag{A15}$$

Taking summation on both sides of (A15) from 0 to k^* yields

$$V(k^*) - V(0) \leq \sum_{k=0}^{k^*} r(w(k), y(k)) - \gamma \sum_{k=0}^{k^*} w^{\mathrm{T}}(k) w(k). \tag{A16}$$

Under the zero initial condition $V(0) = 0$, we have

$$\sum_{k=0}^{k^*} r(w(k), y(k)) \geq \gamma \sum_{k=0}^{k^*} w^{\mathrm{T}}(k) w(k). \tag{A17}$$

For any $k^* > 0$, we can conclude that (18) and (19) holds, which means system (14) is strictly (U_1, U_2, U_3)-γ-dissipative. This completes the proof. □

Appendix B

Proof of Theorem 2. Define

$$\tilde{\Pi}_1 = \begin{bmatrix} \tilde{\Pi}_1^{11} & * \\ \tilde{\Pi}_1^{21} & \tilde{\Pi}_1^{22} \end{bmatrix}, \ \tilde{\Pi}_1^{21} = \begin{bmatrix} \tilde{\Phi}_1^T & \mathbf{0}_{2\varsigma\times 4} & \tilde{\Phi}_2^T \\ \tilde{\Phi}_3^T & \mathbf{0}_{3\varsigma\times 4} & \mathbf{0}_{3\varsigma\times N} \end{bmatrix}^T, \tag{A18}$$

where

$$\tilde{\Pi}_1^{11} = \Pi_1^{11}, \ \tilde{\Pi}_1^{22} = \Pi_1^{22}, \ \mathcal{K}_1 = \left[\bar{B}(K_{\mathrm{I}} - K_{\mathrm{D}})\bar{C}, \ \bar{B}K_{\mathrm{I}}\bar{C}, \ \ldots, \ \bar{B}K_{\mathrm{I}}\bar{C} \right]$$

$$\tilde{\Phi}_1 = \begin{bmatrix} P(\bar{A} + \bar{B}(K_{\mathrm{D}} + K_{\mathrm{P}})\bar{C}) \\ \sqrt{\varepsilon_1}(P(\bar{A} + \bar{B}(K_{\mathrm{D}} + K_{\mathrm{P}})\bar{C})) \end{bmatrix}, \ \tilde{\Phi}_3 = \begin{bmatrix} P\mathcal{K}_1 & P\bar{A}_\tau \\ \sqrt{\varepsilon_1}\mathcal{K}_1 & \sqrt{\varepsilon_1}P\bar{A}_\tau \end{bmatrix}, \ \tilde{\Phi}_2 = \begin{bmatrix} (-U_1)^{\frac{1}{2}}\bar{C} \\ (-U_2)^{\frac{1}{2}}\bar{C} \end{bmatrix}.$$

To eliminate uncertainty $F(k)$, two matrices are given as

$$V = \begin{bmatrix} \mathbf{0}_{5\times 2N} & \mathbf{0}_{5\times 4N} \\ V_{21} & \mathbf{0}_{2\varsigma\times 4N} \\ \mathbf{0}_{4\varsigma\times 2N} & V_{32} \\ \mathbf{0}_{1\times 2N} & \mathbf{0}_{1\times 4N} \end{bmatrix}, \ W = \begin{bmatrix} W_{11} & \mathbf{0}_{4N\times 3\varsigma} \\ W_{21} & W_{22} \end{bmatrix}, \tag{A19}$$

where

$$W_{21} = \begin{bmatrix} \mathbf{0}_{N\times\varsigma} & \daleth_2\bar{C} \\ \mathbf{0}_{N\times\varsigma} & \daleth_3\bar{C} \end{bmatrix}, \ W_{22} = \begin{bmatrix} \daleth_2\bar{C} & \daleth_2\bar{C} & \mathbf{0}_{N\times\varsigma} \\ \mathbf{0}_{N\times\varsigma} & \mathbf{0}_{N\times\varsigma} & \mathbf{0}_{N\times\varsigma} \end{bmatrix}, \ W_{11}^{\mathrm{T}} = \begin{bmatrix} (\daleth_3\bar{C})^{\mathrm{T}} & (\daleth_1\bar{C})^{\mathrm{T}} & (\daleth_1\bar{C})^{\mathrm{T}} & (\daleth_3\bar{C})^{\mathrm{T}} \\ (\daleth_2\bar{C})^{\mathrm{T}} & -(\daleth_3\bar{C})^{\mathrm{T}} & \mathbf{0}_{\varsigma\times N} & \mathbf{0}_{\varsigma\times N} \end{bmatrix}$$

$$V_{32} = \mathrm{diag}\left\{ \sqrt{\breve{\alpha}}P\bar{B}\Xi, \ \sqrt{\breve{\lambda}}P\bar{B}\Xi, \ \sqrt{\breve{\beta}}P\bar{B}\Xi, \ \sqrt{\bar{\lambda}}P\bar{B}\Xi \right\}, \ V_{21} = \begin{bmatrix} \bar{\alpha}P\bar{B}\Xi & \bar{\lambda}P\bar{B}\Xi \\ \sqrt{\varepsilon_1}\bar{\alpha}P\bar{B}\Xi & \sqrt{\varepsilon_1}\bar{\lambda}P\bar{B}\Xi \end{bmatrix}.$$

Therefore, Formula (18) can be rewritten as

$$\tilde{\Pi}_1 + VF(k)W + W^{\mathrm{T}}F^{\mathrm{T}}(k)V^{\mathrm{T}} < 0, \tag{A20}$$

Formula (A20) is equivalent to (A21) based on Lemma 1

$$\tilde{\Pi}_1 + \eta VV^{\mathrm{T}} + \eta^{-1}W^{\mathrm{T}}W < 0, \tag{A21}$$

and Formula (A22) is equivalent to (A21) by the Schur complement

$$\bar{\Pi}_1 = \begin{bmatrix} \bar{\Pi}_1^{11} & * \\ \bar{\Pi}_1^{21} & \bar{\Pi}_1^{22} \end{bmatrix} < 0, \tag{A22}$$

where

$$\bar{\Pi}_1^{11}=\begin{bmatrix}\Gamma_1 & * \\ \Gamma_2 & \Gamma_3\end{bmatrix},\ \bar{\Pi}_1^{21}=\begin{bmatrix}\bar{\Phi}_1^{\mathrm{T}} & \bar{\Phi}_2^{\mathrm{T}} & \bar{\Phi}_3^{\mathrm{T}} \\ \mathbf{0}_{3\varsigma\times 2N} & \mathbf{0}_{3\varsigma\times 2N} & \bar{\Phi}_4^{\mathrm{T}}\end{bmatrix}^{\mathrm{T}},\ \bar{\Phi}_1=\begin{bmatrix}\daleth_3\bar{C} & \daleth_2\bar{C} \\ \daleth_1\bar{C} & -\daleth_3\bar{C}\end{bmatrix},\ \bar{\Phi}_2=\begin{bmatrix}\daleth_1\bar{C} & \mathbf{0}_{N\times\varsigma} \\ \daleth_3\bar{C} & \mathbf{0}_{N\times\varsigma}\end{bmatrix}$$
$$\Gamma_2=\tilde{\Pi}_1^{21},\ \Gamma_3=\tilde{\Pi}_1^{22},\ \Gamma_1(1,1)=\mathcal{P},\ \Gamma_1(2,2)=-Q,\ \Gamma_1(3,3)=-R,\ \bar{\Pi}_1^{22}=\mathrm{diag}\{-\eta\boldsymbol{I}_{N\times N}\}_6$$
$$\bar{\Phi}_4=\begin{bmatrix}\daleth_2\bar{C} & \daleth_2\bar{C} & \mathbf{0}_{N\times\varsigma} \\ \mathbf{0}_{N\times\varsigma} & \mathbf{0}_{N\times\varsigma} & \mathbf{0}_{N\times\varsigma}\end{bmatrix},\ \bar{\Phi}_3=\begin{bmatrix}\mathbf{0}_{N\times\varsigma} & \daleth_2\bar{C} \\ \mathbf{0}_{N\times\varsigma} & \daleth_3\bar{C}\end{bmatrix},\ \mho=\begin{bmatrix}\mathrm{diag}(X)_{11} & \mathbf{0}_{11\varsigma\times 7N} \\ \mathbf{0}_{7N\times 11\varsigma} & \boldsymbol{I}_{7N\times 7N}\end{bmatrix}.$$

In the following steps, we will design the control feedback gains of system (14). Define $\hat{P}=X^{\mathrm{T}}PX$, $\hat{A}=X^{\mathrm{T}}AX$, $\hat{U}_2=X^{\mathrm{T}}C^{\mathrm{T}}U_2X$. Pre- and postmultiply both sides of (A22) by $\mho$ and its transposition. Pre- and postmultiply both sides of (19) by $\mathrm{diag}\{\boldsymbol{I}_{N\times N}, P\}$. This is how (20) and (21) can be obtained.

Define

$$Y_{\mathrm{P}}=K_{\mathrm{P}}\bar{C}X,\ Y_{\mathrm{I}}=K_{\mathrm{I}}\bar{C}X,\ Y_{\mathrm{D}}=K_{\mathrm{D}}\bar{C}X,\ \mathcal{Y}=\Big[(Y_I-Y_D),\ Y_I,\ \ldots,\ Y_I\Big], \tag{A23}$$

based on the above definition of $Y_{\mathrm{P}}=K_{\mathrm{P}}\bar{C}X$, $Y_{\mathrm{I}}=K_{\mathrm{I}}\bar{C}X$, $Y_{\mathrm{D}}=K_{\mathrm{D}}\bar{C}X$, there exists difficulty to obtain K_{P}, K_{I}, and K_{D} directly because the matrix C is not invertible. By defining $N_{\mathrm{P}}\bar{C}=K_{\mathrm{P}}\bar{C}X$, $N_{\mathrm{I}}\bar{C}=K_{\mathrm{I}}\bar{C}X$, $N_{\mathrm{D}}C=K_{\mathrm{D}}\bar{C}X$, and $M_1\bar{C}=\bar{C}X$, refer to the method in [39]. The above problem can be solved by transforming it into the W-problem. We obtain $(M_1\bar{C}-\bar{C}X)^{\mathrm{T}}(M_1\bar{C}-\bar{C}X)=0$, according to the method in [40]. By using the Schur complement, we have the following optimization problem:

$$\begin{bmatrix}-\epsilon\,\boldsymbol{I}_{\varsigma\times\varsigma} & * \\ M_1\bar{C}-\bar{C}X & -\boldsymbol{I}_{N\times N}\end{bmatrix}, \tag{A24}$$

where ϵ is a small enough positive scalar. What is obtained from matrix $\bar{C}$ is the full row rank, that is, matrix M_1 is full rank and invertible. Therefore, we can design control gains K_{P}, K_{I}, and K_{D} on the following results. Then, the system (14) is strictly (U_1,U_2,U_3)-γ-dissipative, and the feedback gains are obtained as $K_{\mathrm{P}}=N_{\mathrm{P}}{M_1}^{-1}$, $K_{\mathrm{I}}=N_{\mathrm{I}}{M_1}^{-1}$, $K_{\mathrm{D}}=N_{\mathrm{D}}{M_1}^{-1}$. The proof of Theorem 2 is complete. □

References

1. Pandey, S.K.; Mohanty, S.R.; Kishor, N. A literature survey on LFC for conventional and distribution generation power systems. *Renew. Sustain. Energ. Rev.* **2013**, *25*, 318–334. [CrossRef]
2. Wang, Q.; Yu, Y.; Zhang, Z.; Han, X. Melnikov-threshold-triggered mixed-mode oscillations in a family of amplitude-modulated forced oscillator. *J. Low Freq. Noise Vib. Act. Control* **2019**, *38*, 377–387. [CrossRef]
3. Yu, Y.; Wang, Q.; Bi, Q.; Lim, C.W. Multiple-s-shaped critical manifold and jump phenomena in low frequency forced vibration with amplitude modulation. *Int. J. Bifurcat. Chaos* **2019**, *29*, 1930012. [CrossRef]
4. Sun, L.; Zhang, C.; Yu, Y. A boundary knot method for 3D time harmonic elastic wave problems. *Appl. Math. Lett.* **2020**, *104*, 106210. [CrossRef]
5. Li, Y.; Ni, Z.; Zhao, T.; Yu, M.; Liu, Y.; Wu, L.; Zhao, Y. Coordinated scheduling for improving uncertain wind power adsorption in electric vehicles-wind integrated power systems by multiobjective optimization approach. *IEEE Trans. Ind. Appl.* **2020**, *56*, 2238–2250. [CrossRef]
6. Nguyen, N.; Mitra, J. An analysis of the effects and dependency of wind power penetration on system frequency regulation. *IEEE Trans. Sustain. Energy* **2016**, *7*, 354–363. [CrossRef]
7. Li, M.; Yang, M.; Yu, Y.; Lee, W.J. A wind speed correction method based on modified hidden Markov model for enhancing wind power forecast. *IEEE Trans. Ind. Appl.* **2022**, *58*, 656–666. [CrossRef]
8. Liao, K.; Lu, D.; Wang, M.; Yang, J. A low-pass virtual filter for output power smoothing of wind energy conversion systems. *IEEE Trans. Ind. Electron.* **2022**, *69*, 12874–12885. [CrossRef]
9. Sun, S.; Liu, Y.; Li, Q.; Wang, T.; Chu, F. Short-term multi-step wind power forecasting based on spatio-temporal correlations and transformer neural networks. *Energy Convers. Manag.* **2023**, *283*, 116916. [CrossRef]
10. Wang, Y.; Meng, J.; Zhang, X.; Xu, L. Control of PMSG-based wind turbines for system inertial response and power oscillation damping. *IEEE Trans. Sustain. Energy* **2015**, *6*, 565–574. [CrossRef]

11. Chen, C.; Su, Y.; Yang, T.; Huang, Z. Virtual inertia coordination control strategy of DFIG-based wind turbine for improved grid frequency response ability. *Electr. Power Syst. Res.* **2023**, *216*, 109076. [CrossRef]
12. Vachirasricirikul, S.; Ngamroo, I. Robust LFC in a smart grid with wind power penetration by coordinated vehicle-to-grid control and frequency controller. *IEEE Trans. Smart Grid* **2014**, *5*, 371–380. [CrossRef]
13. Shangguan, X.C.; Zhang, C.K.; He, Y.; Jin, L.; Jiang, L.; Spencer, J.W.; Wu, M. Robust LFC for power system considering transmission delay and sampling period. *IEEE Trans. Ind. Inform.* **2021**, *17*, 5292–5303. [CrossRef]
14. Peng, C.; Li, J.; Fei, M. Resilient event-Triggering H_∞ LFC for multi-Area power systems with energy-limited DoS attacks. *IEEE Trans. Power Syst.* **2017**, *32*, 4110–4118. [CrossRef]
15. Bevrani, H.; Hiyama, T. Robust decentralised PI based LFC design for time delay power systems. *Energy Convers. Manag.* **2008**, *49*, 193–204. [CrossRef]
16. Ang, K.H.; Chong, G.; Li, Y. PID control system analysis, design, and technology. *IEEE Trans. Control Syst. Technol.* **2005**, *13*, 559–576.
17. Singh, V.P.; Kishor, N.; Samuel, P. Improved LFC of power system using LMI based PID approach. *J. Frankl. Inst.* **2017**, *354*, 6805–6830. [CrossRef]
18. Pradhan, J.K.; Ghosh, A. Multi-input and multi-output PID controller design via linear quadratic regulator-linear matrix inequality approach. *IET Control Theory Appl.* **2015**, *9*, 2140–2145. [CrossRef]
19. Pandey, S.K.; Kishor, N.; Mohanty, S.R. Frequency regulation in hybrid power system using iterative PID H_∞ controller. *Electr. Power Compon. Syst.* **2014**, *42*, 132–148. [CrossRef]
20. Zhong, Q.; Yang, J.; Shi, K.; Zhong, S.; Li, Z.; Sotelo, M.A. Event-triggered H_∞ LFC for multi-area nonlinear power systems based on non-fragile proportional integral control strategy. *IEEE Trans. Intell. Transp. Syst.* **2022**, *23*, 12191–12201. [CrossRef]
21. Elsisi, M.; Soliman, M. Optimal design of robust resilient automatic voltage regulators. *ISA Trans.* **2021**, *108*, 257–268. [CrossRef] [PubMed]
22. Wang, Y.; Zou, L.; Zhao, Z.; Bai, X. H_∞ fuzzy PID control for discrete time-delayed T-S fuzzy systems. *Neurocomputing* **2019**, *332*, 91–99. [CrossRef]
23. Zhao, D.; Wang, Z.; Wei, G.; Han, Q.L. A dynamic event-triggered approach to observer-based PID security control subject to deception attacks. *Automatica* **2020**, *120*, 109128. [CrossRef]
24. Shen, H.; Xing, M.; Xu, S.; Basin, M.V.; Park, J.H. H_∞ stabilization of discrete-time nonlinear semi-Markov jump singularly perturbed systems with partially known semi-Markov Kernel information. *IEEE Trans. Circuits Syst. I Reg. Pap.* **2021**, *68*, 818–828. [CrossRef]
25. Feng, Z.; Lam, J.; Gao, H. α-Dissipativity analysis of singular time-delay systems. *Automatica* **2011**, *47*, 2548–2552. [CrossRef]
26. Bullo, F. Averaging and vibrational control of mechanical systems. *SIAM J. Control Optim.* **2002**, *41*, 542–562. [CrossRef]
27. Fantoni, I.; Lozano, R.; Spong, M. Energy based control of the Pendubot. *IEEE Trans. Autom. Control* **2000**, *45*, 725–729. [CrossRef]
28. Wang, Y.; Cheng, D.; Li, C.; Ge, Y. Dissipative Hamiltonian realization and energy-based L_2-disturbance attenuation control of multimachine power systems. *IEEE Trans. Autom. Control* **2003**, *48*, 1428–1433. [CrossRef]
29. Galaz, M.; Ortega, R.; Bazanella, A.S.; Stankovic, A.M. An energy-shaping approach to the design of excitation control of synchronous generators. *Automatica* **2003**, *39*, 111–119. [CrossRef]
30. Wu, Z.G.; Shi, P.; Su, H.; Chu, J. Dissipativity Analysis for Discrete-Time Stochastic Neural Networks With Time-Varying Delays. *IEEE Trans. Neural Netw. Learn. Syst.* **2013**, *24*, 345–355. [CrossRef]
31. Wang, J.; Huang, Z.; Wu, Z.; Cao, J.; Shen, H. Extended dissipative control for singularly perturbed PDT switched systems and its application. *IEEE Trans. Circuits Syst. I Reg. Pap.* **2020**, *67*, 5281–5289. [CrossRef]
32. Feng, Z.; Lam, J. Stability and dissipativity analysis of distributed delay cellular neural networks. *IEEE Trans. Neural Netw. Learn. Syst.* **2011**, *22*, 976–981. [CrossRef]
33. Meisami-Azad, M.; Mohammadpour, J.; Grigoriadis, K.M. Dissipative analysis and control of state-space symmetric systems. *Automatica* **2009**, *45*, 1574–1579. [CrossRef]
34. Willems, J.C. Dissipative dynamical systems part I: General theory. *Arch. Ration. Mech. Anal.* **1972**, *45*, 321–351. [CrossRef]
35. Peng, C.; Zhang, J.; Yan, H. Adaptive event-triggering H_∞ LFC for network-based power systems. *IEEE Trans. Ind. Electron.* **2018**, *65*, 1685–1694. [CrossRef]
36. Jin, L.; He, Y.; Zhang, C.K.; Shangguan, X.C.; Jiang, L.; Wu, M. Novel structure-exploiting techniques based delay-dependent stability analysis of multi-area LFC with improved numerical tractability. *IEEE Trans. Power Syst.* **2021**, *36*, 4194–4211. [CrossRef]
37. Li, T.; Guo, L.; Sun, C. Robust stability for neural networks with time-varying delays and linear fractional uncertainties. *Neurocomputing* **2007**, *71*, 421–427. [CrossRef]
38. Jin, L.; He, Y.; Zhang, C.K.; Shangguan, X.C.; Jiang, L.; Wu, M. Robust delay-dependent LFC of wind power system based on a novel reconstructed model. *IEEE Trans. Cybern.* **2021**, *52*, 7825–7836. [CrossRef]
39. Crusius, C.; Trofino, A. Sufficient LMI conditions for output feedback control problems. *IEEE Trans. Autom. Control* **1999**, *44*, 1053–1057. [CrossRef]
40. Peng, C.; Zhang, J. Delay-distribution-dependent LFC of power systems with probabilistic interval delays. *IEEE Trans. Power Syst.* **2016**, *31*, 3309–3317. [CrossRef]